THE FIRST USV FLIGHT TEST

G. Russo

CIRA, Italian Aerospace Research Center,
81043 Capua,
Italy

ABSTRACT

The first Dropped Transonic Flight Test of USV (Unmanned Space Vehicles), performed with **Castor**, the first of the two spacecrafts developed within the USV Program, was performed on Saturday 24th February 2007, from Tortolì Airport in Sardinia.

At 8:30 a.m. the 340000 cubic meters stratospheric balloon lifted off from the East coast of Sardinia, bringing the Flying Test Bed up to 20.2 km before release within the isolated sea polygon controlled by Italian Air Force Fire Test Range in Salto di Quirra (PISQ). The mission ended at 10:30 a.m. with the splash-down of the space vehicle.

The flight itself was very good, with a nose-up manoeuvre under transonic conditions, reaching a maximum Mach as high as 1.08. The mission target was completely achieved as some 2 million measures were taken related to flight data, housekeeping, as well as 500 aerodynamic and structural experimental sensors. Unfortunately, the vehicle has been damaged more than expected during splash down.

Many national and international institutions and industries contributed to the mission carrying out, under the supervision and technical guide of CIRA: Italian Space Agency, Italian Air Force, Italian Navy, Italian Civil Aviation Authority, Italian Company for Air Navigation Services, Port Authorities, European Space Agency, Techno System Dev., Vitrociset, Carlo Gavazzi Space, Space Software Italia, Alcatel Alenia Space Italy, ISL-Altran Group).

The paper will report the flight data analysis as well as lessons learned and expected evolution of the PRORA-USV Program.

1. INTRODUCTION

The USV Program is a technology program aimed at developing a family of multi-purpose FTBs able to execute atmospheric re-entry from low earth orbit (LEO). The first phase of the USV Program foresees the realization of two units of the first flying platform, FTB_1, addressing low atmosphere maneuvered missions under subsonic, transonic and low supersonic regimes. The vehicle is launched by means of a stratospheric balloon and released at an altitude between 20 and 35 km.

The second phase of the USV Program aims at the development and operation of an advanced flying laboratory, FTB_X, oriented towards advanced missions covering all the atmospheric re-entry flight regimes, until a final re-entry from LEO mission. The FTB_X is designed to be launched from the ESA-GSC in Kourou using the VEGA launcher.

In the frame of the first phase of the program, a series of missions of increasing complexity has been planned, the first of which is the Dropped Transonic Flight Test (DTFT). It is mainly aimed at testing the aerodynamics and flight behavior in transonic flight regime, in a condition similar to that experienced by a winged launcher stage during its atmospheric re-entry trajectory.

The design of the DTFT is based on using a two-stage system that is composed by an expendable first stage, a carrier based on a stratospheric balloon, and the winged re-entry flight test bed (FTB_1 vehicle), as the second stage. The nominal mission profile of DTFT is schematically depicted in Fig. 1 and can be summarised as follows.

The basic operations consist of three main phases:

- the ascent phase, from lift-off to the vehicle release (around 20 km altitude), during which the carrier system brings FTB_1 to the target altitude by means of the stratospheric balloon;
- the flight phase, from vehicle release to parachute opening, when FTB_1 is detached from the carrier and flies accelerating to achieve the required velocity to perform the experiments. In this phase FTB_1 passes through the transonic regime (the maximum Mach number is around 1.1), between 10 and

15 km, in stabilized attitude while performing an autonomous aero-controlled flight;

– the deceleration phase, from parachute opening to splashdown, in which FTB_1 opens the parachute and the mission ends with the sea splashdown and successive recovery.

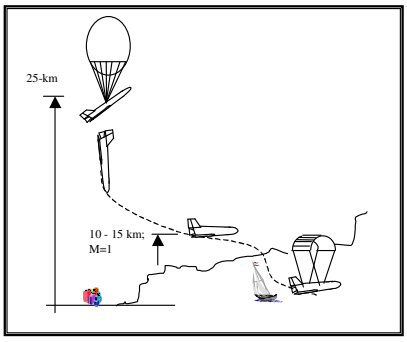

Figure 1. DTFT mission scheme

The first DTFT was carried out on 24th February 2007 from Arbatax in Sardegna, Italy.

At 8:30 a.m. the 340000 cubic meters stratospheric balloon lifted off from the East coast of Sardinia, bringing the Flying Test Bed up to 20.2 km before release within the isolated sea polygon controlled by Italian Air Force Fire Test Range in Salto di Quirra (PISQ). The mission ended at 10:30 a.m. with the splash-down of the space vehicle.

The flight itself was very good, with a nose-up manoeuvre under transonic conditions, reaching a maximum Mach as high as 1.07. The mission target was completely achieved as some 2 million measures were taken related to flight data, housekeeping, as well as 500 aerodynamic and structural experimental sensors. Unfortunately, the vehicle has been damaged more than expected during splash down.

Many national and international institutions and industries contributed to the mission carrying out, under the supervision and technical guide of CIRA: Italian Space Agency, Italian Air Force, Italian Navy, Italian Civil Aviation Authority, Italian Company for Air Navigation Services, Port Authorities, European Space Agency, Techno System Dev., Vitrociset, Carlo Gavazzi Space, Space Software Italia, Alcatel Alenia Space Italy, ISL-Altran Group).

The vehicle accommodated onboard a scientific payload (or a Passenger EXperiment, PEX) which was aimed at conducting two main experiments: an aerodynamic test coupled with a structural test for validating the overall aerodynamic and structural design and analysis tools and a GN&C technology test aimed at validating the stability and control augmentation system and related analysis and design tools in the re-entry flight phase of Terminal Area Energy Management (TAEM), which ranges from Mach 2.0 to 0.5.

Furthermore, the DTFT mission allowed to gather significant information regarding the separation from the balloon and the starting phase of the FTB_1 descent; and the capability to cope with the mission final phase, from parachute opening to recovery.

2. SYSTEM LAYOUT AND FLIGHT MISSION

As already mentioned, the entire system consisted of a carrier system, whose function is to drive the vehicle to the desired altitude, and of the vehicle itself. The carrier is made by a structure, which we call *gondola*, connected to the balloon through the launch chain. The gondola houses all the electrical and mechanical equipment devoted to control the ascent flight and to assist the FTB_1 demonstrator in this phase. For instance, the venting valves telecommand and the auxiliary ballast discharge system for the balloon guidance are both located onboard the equipped gondola. The gondola has a dedicated parachute which is integrated between the stratospheric balloon and the gondola itself. This parachute has a twofold purpose, indeed it has to insure a safe termination of the mission in the case of an emergency and the safe descent of the gondola once separation from the vehicle has been accomplished in nominal mode.

The vehicle is mechanically connected to the gondola and is separated from it by means of a separation device.

The FTB_1 demonstrator is a slender, non-propelled, winged vehicle able to perform experiments on structure and materials, autonomous guidance navigation and control, and thermo-aerodynamics.

The needs cited above led to the implementation of an airplane-like configuration for FTB_1 with a main physical structure housing a certain number of subsystems. The external configuration has been developed following the design driving features listed below:

- aerodynamic efficiency of L/D>2.5 from transonic to supersonic regimes
- maximum thickness of wing profile: 8%
- nominal nose radius: < 50 mm
- a four-vertical-fins configuration, in order to reduce interference with wings, with parachute at deployment, and structural constraints, as well as to match stability and control requirements.

The FTB_1 is 9 m long with a weight of 1300 kg. Both systems are depicted in Fig. 2 where one can see the gondola and FTB_1 vehicle linked together and suspended from the launch machine on the

launch pad in Arbatax during the preflight operations.

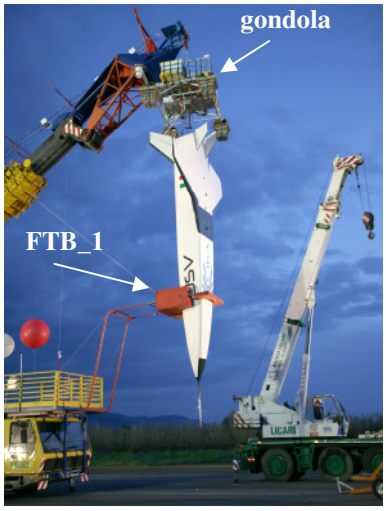

Figure 2. FTB_1 and gondola suspended from the launch machine before flight.

The architecture of the Avionic System for the FTB has been defined by considering the following main requirements:

- Modularity, upgradeability and standardization
- Reliability
- Performances

In the last years, to reduce costs and development time of the Avionic Systems, the Space Programs are strongly requiring the adoption of open, modular, up-gradable and standard bus architecture, recommending also (when it is possible) the use of commercially available products. The same approach has been selected by CIRA for the FTB Avionic System.

The main components of the Avionic System and their connection to the other FTB's subsystems are outlined in Fig. 3.

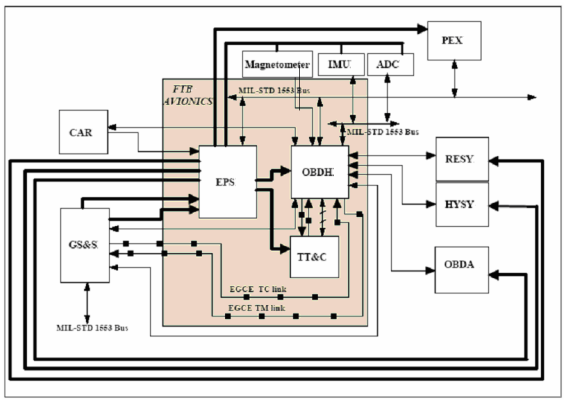

Figure 3. Avionic System Schematic diagram

The mission is schematically shown in the Mach-Altitude plane (Fig. 4), where the main events are indicated.

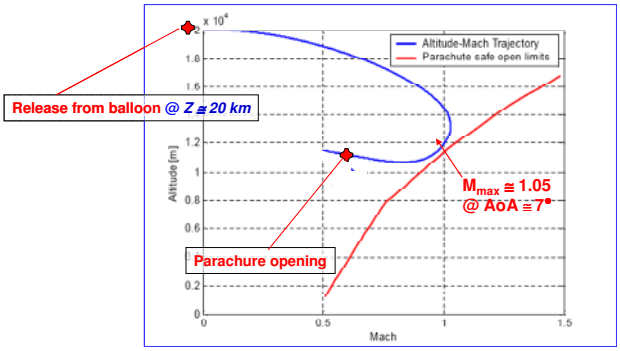

Figure 4. DTFT Mission Schematic

The actual DTFT trajectory and main events are illustrated in Fig. 5.

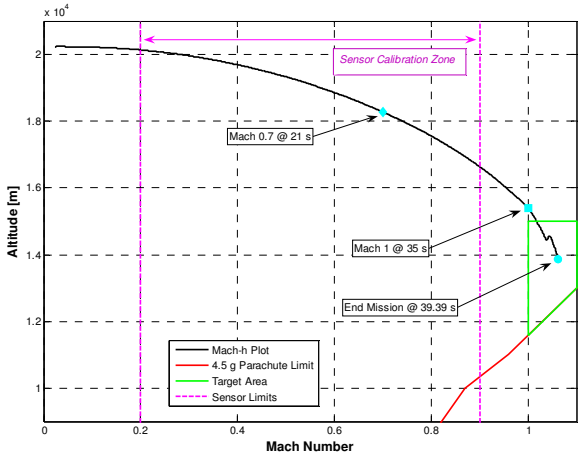

Figure 5. DTFT Actual Mission

3. ON BOARD EXPERIMENTS

3.1. Aerodynamics Test

The main target of the aerodynamics experiment is to provide a database of measurements during flight of body local pressure and flight characteristic parameters in order to support and integrate the CFD models adopted for the vehicle design. Note that this is a challenging task because, as it is well known, in the transonic regime the aerodynamic coefficients are highly varying functions of Mach number and of angle of attack, due to fluid dynamic nonlinearities.

Furthermore, the prediction of the aerodynamic coefficients of FTB_1 was particularly hard as a consequence of the specific geometrical configuration which led to some critical calculations such as base flow, wing/strake interaction, butterfly tail, large fuselage and double ventral fin influence.

Moreover, since there is a large altitude variation, a wide range of Reynolds number is expected over the mission.

In the table below the mission/experiment requirements are reported in terms of the aerodynamic parameters range and their profile.

	Profile	Range	Notes
Mach	Sweep	from 0.7 to 1.07	Acceleration/ decelaration
Reynolds	f(M,z)	[1E6;1E7]	
AoA	Constant	≥ 4°	
Sideslip	Constant	0°	Longitudinal symmetric flight

Table 1. Aerodynamic parameters requirements.

Hence, the experiment focuses on the evaluation of the Mach number effect on the longitudinal aerodynamic coefficients over the descending flight at constant angle of attack, and, at the same time, on the influence of Reynolds number (by means of the different altitudes swept). In doing so, the main parameter of interest, apart from the global aerodynamic data, is the surface static pressure. A comparison between the measured and predicted distributions along the trajectory is useful for verification.

A pitot boom system was installed on the metallic nose of the vehicle (Fig. 6) in order to measure the free stream thermodynamic data along with total pressure and temperature and both the angles of attach and sideslip. These data allowed to determine completely the aerodynamic conditions.

The regions where pressure taps have been installed were identified as the areas of expected strong pressure gradients. The pressure coefficient contours over the body, shown in Fig. 5, allows a direct evaluation of these zones which are highlighted with yellow arrows.

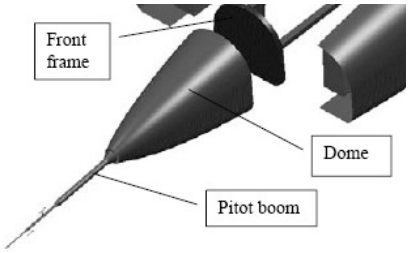

Figure 6. Pitot boom location on the vehicle.

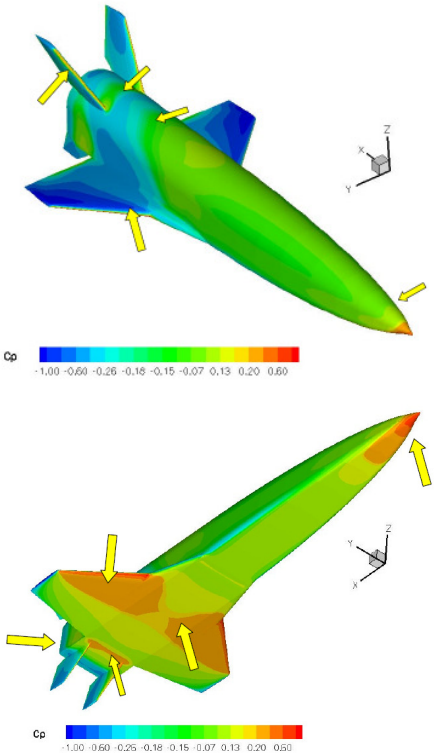

Figure 7. Calculated pressure coefficient contours (M=1.05, Re=7.8E6, AoA=10°, AoS=0°).

A total of 304 pressure taps were then installed in the areas reported in the following:

- NOSE
- WING (maximum pressure variation and shock waves expected in transonic regime)
- FIN (fluid dynamic interference likely)
- MID FUSE
- REAR FUSE
- BASE PLATE (flow separation and recirculation).

A layout of the pressure taps located over the right wing is sketched in the figure below.

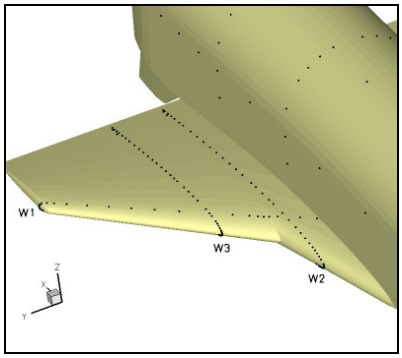

Figure 8. Pressure taps layout.

Pressure was measured by means of miniaturized piezoelectric pressure transducers encapsulated in electronic pressure scanners produced by Scanivalve Corp. The pressure scanner model is ZOC22B which has a full scale of 50 psid and an accuracy of 0.05% F.S and is equipped with a temperature compensation unit. These sensors are specifically designed for use in flight tests where operational conditions are very space-constrained.

3.2. Aero-Structural Tests

Aero-structural experiments made use of two types of sensors data: strain-gages and accelerometers.

A series of strain-gages was employed in order to qualify the structural behaviour of the vehicle and to evaluate the external loads (shear, and moments) in order to validate the theoretical methods for load evaluation.

The accelerometers, on the other hand, were employed to identify typical aeroelastic parameters, such as frequency and damping.

Approximately 100 strain gauges produced by Vishay Intertechnology Inc. were installed on the vehicle structural items.

Also 7 flight piezoelectric accelerometers Endevco model 258A were installed on both sides of the wing, fin tip and front fuselage bulkhead.

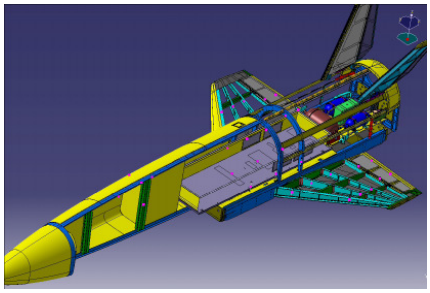

Figure 9. Strain gauges position.

3.3. GN&C Test

Three main objectives were identified for GN&C related technologies for this first DTFT:

- verification of flight mechanics uncertainty models and related control clearance tools;
- validation of design tools and control strategies to obtain the desired aerodynamic test conditions despite the large modeling uncertainties and environmental disturbances;
- demonstration of GN&C rapid prototyping development and verification technologies that will allow to rapidly and safely implement new GN&C algorithms for subsequent missions.

While the last objective was justified by the stringent mission's schedule and the need to demonstrate capabilities for reusability of flying demonstrators, the main critical aspects calling for innovative control clearance technologies and design approaches for the GN&C are the unsteady nature of the tracked reference trajectory, the extreme variability of the flight regimes in which a re-entry vehicle is intended to operate, and the wide uncertainty ranges affecting the design parameters, most notably the aerodynamic characteristics.

Specifically for what concerns uncertainty modeling and clearance methodologies, the conventional flight control law (FCL) robustness analysis methods may become inappropriate or extremely conservative. Thus different approaches have been applied such as Monte Carlo methods, that are customary used at the end of the control laws design loop for formal FCL clearance, but also innovative technologies which can be used during the design phase to drive wind tunnel aerodynamic testing process and control algorithm improvement.

Furthermore, critical aspects specific of a drop test, such as largely uncertain initial conditions and poor controllability of the vehicle at low dynamic pressure 5, also justify the challenge on attitude control strategy to be used during the flight.

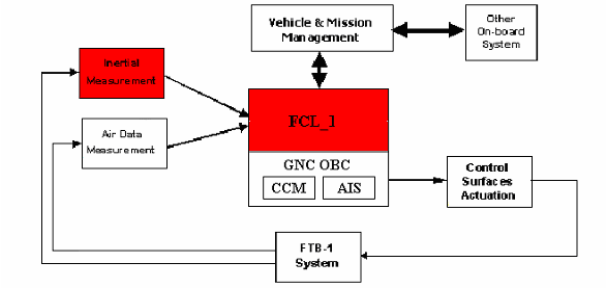

Figure 10. GN&C Architecture.

To be able to perform the DTFT, the GN&C algorithms FCL_1 (including actuator's control loops) were hosted on a dedicated real time computer GNC-OBC interfaced with the on-board data handling computer for obtaining mission phases scheduling information. The GNC system also comprises a dedicated Fiber Optic based INS/GPS unit, a magnetometer and a blow-down hydraulic system for actuation of aerodynamic surfaces. Actually, in order to fulfill aerodynamic test conditions, also the on-board Air Data system measurements have been used.

4. SOME RESULTS

3.1. Aerodynamics

In order to extract from the test the appropriate information to verify the accuracy of the used design tools (a mix of know-how, wind tunnel, CFD and engineering tools) it is necessary to accurately know along the trajectory "flown" the entire set of flight conditions in terms of flight point (altitude, air speed, aircraft attitude), aircraft configuration (control surfaces deflections), aerodynamic forces and measured quantities (surface pressures in the present case).

In fact, starting from this information, it is then possible to rebuild by means of three dimensional Navier-Stokes calculations the real flight conditions and so to validate the used modelling (in terms of computational grid, turbulence model, laminar-turbulent transition, etc.).

Moreover in order to properly synchronize the pressure measurements with the flight point knowledge, whose time shift is due to the dynamic response of the sensors pneumatic lines a SW tool has been properly developed, although it isn't yet validated against experimental tests (still on-going). Furthermore other tests are planned for pressure scanners inside a climatic chamber to characterise the effect of temperature variation during the flight on the sensor accuracy. In the meantime, these corrections, are not yet considered.

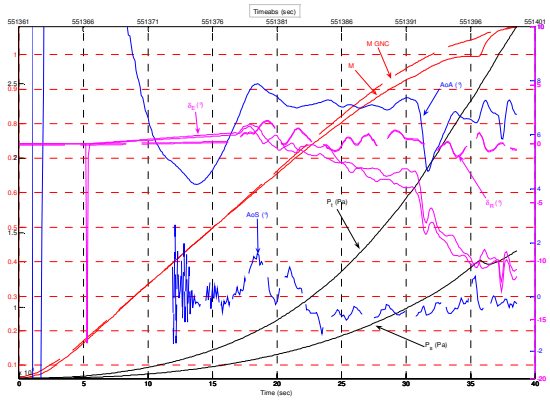

Figure 11. Time behavior of the flight parameters

In Fig. 11 the time behaviour of the flight parameters (M_∞, α, β, P_{tot}, p_∞, δ_{elv}, δ_r) is plotted. All the quantities are referred to the UTC time (from satellite); the test window is of about 38 sec (from t_i=551360 sec to t_f=551400).

In the present preliminary analysis we have focused our attention on the wing section W3 (the Y=1000 mm spanwise section) and on the base plate (BP), judged the most appropriate for the present objective.

The sensor distribution on the W3 section is shown in Fig. 12. The coloured circles indicate the locations on the wing section of the pressure sensor whose temporal measurement is reported in Fig. 13, within the temporal acquisition window; in the same figure also the Mach number and the angle of attack are reported for comparison purposes.

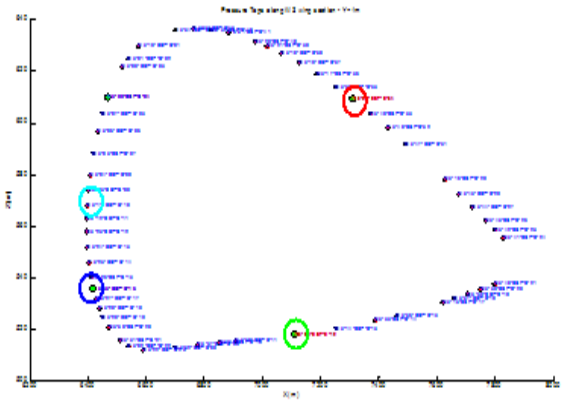

Figure 12. Sensor position on W3 wing section

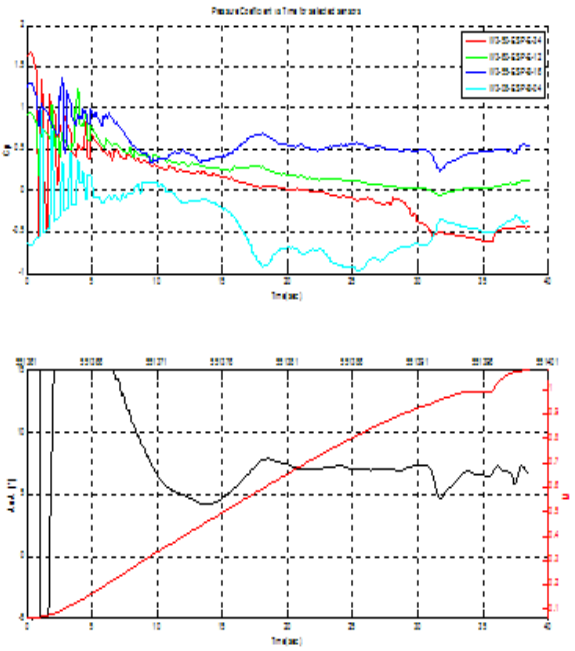

Figure 13. Recorded pressure on W3 wing section

It can be noted that the expansion peak on the leeside and the compression peak on the windside, just behind the stagnation point, still remain almost constant all along the pure high-subsonic flight duration until the sudden variation at t=31 sec is in correspondence of a rapid decrease of the angle of attack from about 7.5 deg to about 5 deg, with the correspondent movement of the stagnation point and the global lift decrease, when the transonic flight starts.

In fig.14 Cp distribution on W3 section is plotted at t=25s, M=0.80, □=7.03°; its behaviour seems globally consistent with the expected distributions. However, these measurements will we verified only through a comparison with the running the CFD reconstructions, based of the actual vehicle geometry (in terms of control surface deflection) known only when the flight was done.

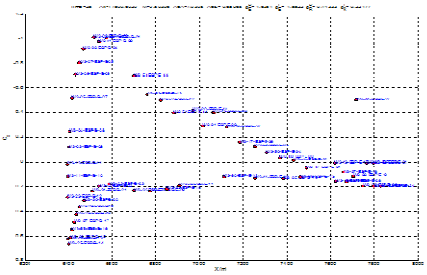

Figure 14. Cp distribution on W3 wing section

Finally, the not symmetrical distribution of the pressure on the base plate BP is reported in the Fig. 15, while the temporal behaviour of the pressure coefficient on BP is on Fig. 16. On the same figure the computed value of the BP pressure coefficient (symbols) is reported; the figure seems to show a consistent course of the three measures valued that seem to converge to an enough constant value of Cp on the BP. Note also in this case the effect of the sudden angle of attack variation recorded at about to t=31 sec of the useful experimentation windows, that determines an increase of the contribution of the base to the drag coefficient.

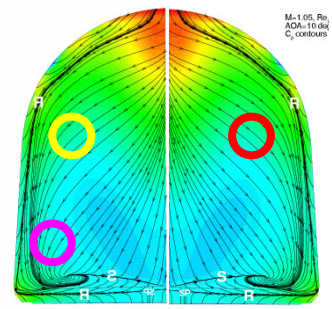

Figure 15. Base plate with the sensors location

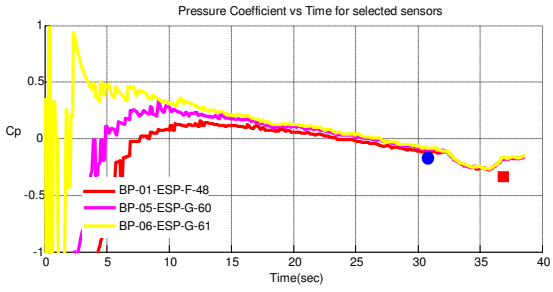

Figure 16. Measured base Cp compared predictions

3.2. Structure

This section is divided in two subsections where the preliminary results of strain-gauge and accelerometers measurements will be analysed respectively.

4.2.1 In Flight Loads Estimation By Strain Gauges Technique

The aim of this experiment is the evaluation of external forces (shears and moments) starting from the deformation measured during flight of FTB_1.

At the moment a method (based on [8]) is under development aiming to translate the internal deformation (με) into external forces due to the aerodynamic field.

This method is essentially based on a linear relationship between strain and applied loads. Briefly, by means of a pre-flight proper calibration, the coefficients of the linear relationship between applied forces and measured strains are evaluated, so that it is possible, by inversion of this relation, to derive loads from strains.

However, at this stage, the consistency of internal deformation has been verified.

Once voltage signals have been transformed into deformations/stress, and preliminary operations have been performed, the acquired data have been plotted (stress vs. time) to have a match with numerical evaluations. The following figures show the data mentioned above related to some of the instrumented wing sections.

Fig. 17 shows the wing stress time history during the controlled mission stage.

In particular, for an up-deflection of the wing, the strains (and consequently the stresses) relative to the spars upper caps are negative (compression zones) while the bottom caps are in tension (positive measured stresses) according to the vehicle attitude. The stress levels are in accordance with the ones evaluated using the FEM simulations.

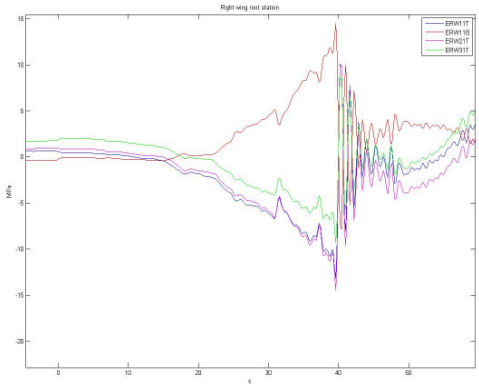

Figure 17. Stresses on caps of right wing root section.

For all items the max stress level is much lower than the material allowable one.

4.2.2 Aeroelastic Parameters Estimation By In Flight Data Acquisition

The aim of this experiment is an estimate of aeroelastic parameters (frequency and damping) of the vehicle subjected to the aerodynamic field.

At the moment a detailed aeroelastic model based on Ground Vibration Tests is being developed (GVT); flight data will allow us to validate this model.

Likewise Loads Evaluation Experiment, a preliminary treatment of the signals from accelerometers has been performed. Figs. 18 and 19 show the 1st symmetrical bending frequency and the 1st anti-symmetrical one detected during flight. The evaluation has been obtained performing the FFT of the symmetric and antisymmetric signals obtained by superposition of left and right wing side accelerometric responses.

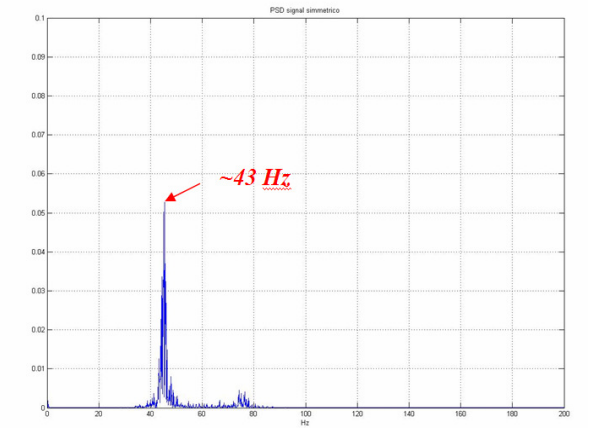

Figure 18. 1st symmetrical bending frequency of wing.

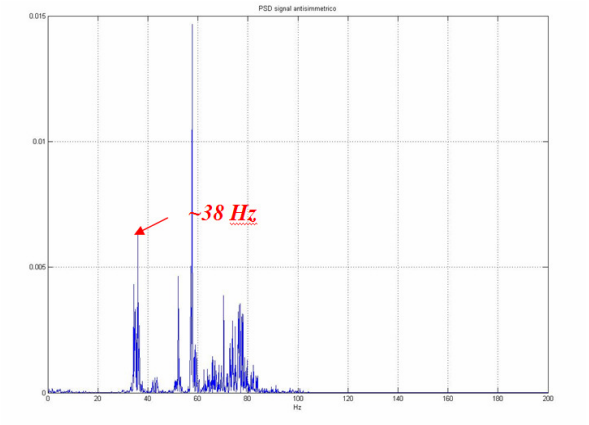

Figure 19. 1st anti-symmetrical bending frequency of wing.

The same frequencies have been evaluated using a dynamic FE model of the vehicle.

The following table shows the consistency between the measured and calculated frequencies.

Characterization	Measured [Hz]	Numerical [Hz]
1st symmetric	~43	38.62
1st anti-symmetric	~38	39.30

Table 2. Comparison between measured and predicted oscillation frequencies.

3.3. GN&C

The controlled flight phase of DTFT can be divided in three main subphases: an initial acceleration subphase in vertical nose down attitude, in which the vehicle is stabilized up to about Mach 0.4 is reached, a transition phase in which a wing levelled pull-up manoeuvre is initiated and a test phase starting from Mach 0.7 with constant angle of attack of 7.5deg and 0deg angle of sideslip until the parachute opening command is issued.

Actually, the DTFT flight phase lasted a total time of about 40 s without any noticeable off-nominal conditions with respect to the above sketched flight timeline, reaching Mach 1.0 at an altitude of 15 km and a maximum Mach number of about 1.07 at an altitude of about 13.5 km, in a controlled aerodynamic attitude. In the following figures the time histories of angle of attack and sideslip are reported evidencing that aerodynamic test conditions have been satisfied.

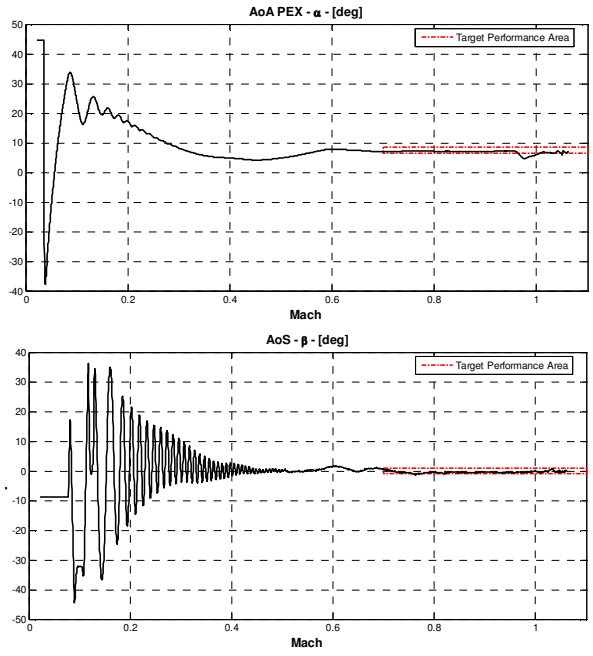

Figure 20. Aerodynamic angles control performance.

A comparison between the measured angle of attack and sideslip and the results of a Monte Carlo analysis performed prior to the DTFT also show that the uncertainty models used for control clearance process are well representative of the actual flight behaviour of the vehicle.

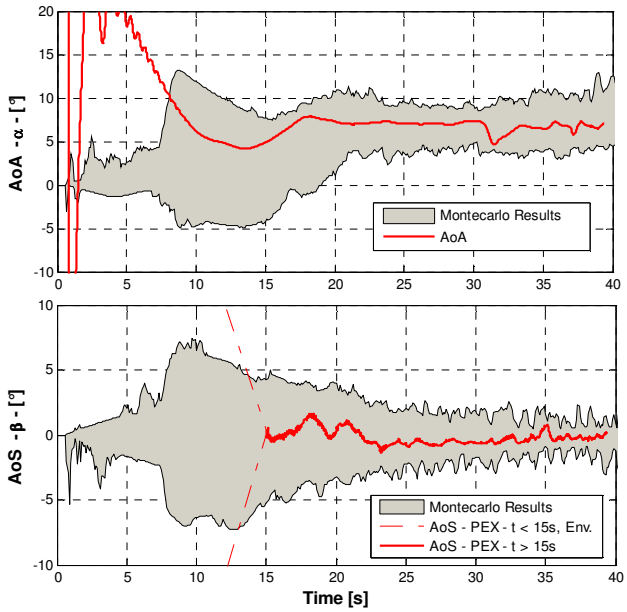

Figure 21. Flight vs. Monte Carlo results.

REFERENCES

1. Russo, G., *Flight Test Experiments Foreseen for USV*, VKI Lecture Series on Flight Experiments for Hypersonic Vehicle Development, Brussels 24-28 October 2005
2. Russo, G., et al., *Unmanned Space Vehicle Program: DTFT In Flight Experiments*, 18th ESA Symposium on European Rocket and Balloon Programmes and Related Research, 3-7 June 2007, Visby Sweden
3. De Matteis, P.P., Corraro, F., Sabatano, R., Russo, G., *DTFT-1: The First Flight of the Automatically Controlled Unmanned Space Vehicle*, 1st International Workshop on "Autonomous Navigation and Artificial Intelligence: state-of-the-art and advances", Pratica di Mare (Italy), July 2007
4. Cobleigh, B. R., *Development of the X-33 Aerodynamic Uncertainty Model*, NASA/TP-1998-206544, 1998
5. Tsukamoto, T., Suzuki, H., *Guidance and Control Design for HOPE-X High Speed Flight Demonstrator Phase II*, AIAA 10th International Space Planes and Hypersonic Systems and Technologies Conference, Japan 2001
6. Corraro, F., Filippone, E., Russo, M., Morani, G., *A Monte Carlo Based Analysis for USV FTB1 DTFT Mission Validation*, AIAA/AHI 14th International Space Planes and Hypersonics Systems and Technologies Conference, Australia 2006
7. Tancredi, U., Grassi, M., Corraro, F., Filippone, E., Palumbo, R., Russo, M., *A Novel Method For Flight Control Laws Robustness Analysis Over Unsteady Trajectories*, accepted for presentation to IFAC-ACA 2007
8. Skopinski T.H,. Aiken Jr W. S. and Huston W. B., *Calibration of strain-gage installation in aircraft structures for the measurements of flight loads*, NASA Technical Report 1178, 1953.